NJC

Visible-light driven electrochemical biofuel cell with the function of CO_2 conversion to formic acid coupled thylakoid from microalgae and biocatalyst immobilized electrodes

Journal:	*New Journal of Chemistry*
Manuscript ID	NJ-ART-03-2018-001118.R1
Article Type:	Paper
Date Submitted by the Author:	17-Apr-2018

Complete List of Authors:	Amao, Yutaka; Osaka City University, Advanced Research Institute for Natural Science and Technology; Osaka City University, Research Center for Artificial Photosynthesis Fujimura, Miyuki; Osaka City University Miyazaki, Makiko; Osaka City University, Advanced Research Institute for Natural Science and Technology Tadokoro, Akemi; Oita University Nakamura, Miki; Oita University Naho, Shuto; Oita University,

Journal Name

ARTICLE

Visible-light driven electrochemical biofuel cell with the function of CO_2 conversion to formic acid coupled thylakoid from microalgae and biocatalyst immobilized electrodes

Received 00th January 20xx,
Accepted 00th January 20xx

DOI: 10.1039/x0xx00000x

www.rsc.org/

Y. Amao[a,b,d]*, M. Fujimura[a,d], M. Miyazaki[a,d], A. Tadokoro[c,d], M. Nakamura[c,d] and N. Shuto[c,d]

Aerobic photosynthesis in green plants, cyanobacteria, and micro-algae has two important sites in the integral-membrane photoactive complexes, photosystems I (PSI) and II (PSII). These systems are assembled into thylakoid membranes. Thylakoid membranes with oxygen-evolution activity owing to PS II can be used in a visible-light driven water photolytic material. In this work, a new visible-light driven electrochemical biofuel-based cell consisting of thylakoid membrane from microalgae *Spirulina platensis* immobilized on a nanocrystalline TiO_2 layer electrode as a photoanode, formate dehydrogenase (FDH)/viologen co-immobilized electrode as a cathode, and CO_2-saturated buffer solution as the redox electrolyte, was developed. The actual short-circuit photocurrent of this cell was estimated to be *ca.* 50 μAcm^{-2}. Formic acid and oxygen were produced in this biofuel cell, while generating electricity from irradiated visible light. The ratio of formic acid to oxygen produced in the biofuel cell after continuous irradiation was estimated to be ~ 2. Thus, formic acid and oxygen was produced stoichiometrically in this visible-light driven electrochemical biofuel cell. Thus, a new biofuel cell system with functions of a solar cell and ability of CO_2 conversion was developed.

Introduction

Green plants, cyanobacteria, and micro-algae use an aerobic photosynthesis system to convert solar light energy into chemical materials such as starch. [1] An aerobic photosynthesis system uses a water molecule as an electron donor. In general, an aerobic photosynthesis system consists of two photosystem sites in the thylakoid membrane (TK) photoactive complexes: photosystem I (PSI) and photosystem II (PSII). [2-4] PSI facilitates the photoreduction of $NADP^+$ to NADPH with P700 reaction center complex. PSII serves as the reaction center with P680 for oxygen production due to water photo-oxidation, including oxygen-evolving complex protein (OEC). Thus, thylakoid membrane is an attractive material for visible-light driven photolysis of water into oxygen and hydrogen gases, combination of hydrogen producing catalyst such as hydrogenase. Especially, some studies on the visible-light driven hydrogen production with the combination system of PSI and hydrogenase or platinum nanoparticle.[5-7] Recently, many studies on biomimetic photovoltaic conversion systems using photosynthetic pigments such as chlorophyll, its derivative, or artificial dyes in assembling the electrode have been reported. [8-21] We developed the photovoltaic conversion system using light-harvesting antenna complex II (LHCII) isolated from a green plant, spinach, immobilized onto nanocrystalline TiO_2 electrode. [22] As PSII is an attractive material for visible-light driven photolysis of water into oxygen, some studies on the photovoltaic conversion system using purified-PSII assembled onto electrode have been reported.[23-31] Willner et al. reported the integrated PSII-based photo-bioelectrical cells with bilirubin oxidase (BOD) immobilized carbon nanotube electrode.[26] PSII also is attractive material for the photo-bioelectrical cell with the semiconductor-based photocatalysis such as TiO_2 electrode. As the PSII purified from *Spinach* or micro-algae is very unstable, however, stability against light irradiation for a long period and on the electrode are serious problems for the utilization of photovoltaic conversion device. Moreover, PSII alone will also not work with TiO_2 because the conduction band of TiO_2 (-0.6 eV vs NHE pH 7.0) is at higher potential than those of P680*, the excited state of reaction center P680 in PSII (-0.58 V vs NHE pH 7.0) and quinone derivative, the last mediator in the electron transfer chain in PSII (redox potential: -0.03 V vs NHE pH 7.0), disabling the direct electron transfer from PSII to TiO_2. [30] On the other hand, the redox potential of P700*, the excited state of reaction center P700 in PSI is estimated to be -1.30 V (vs NHE pH 7.0). Thus, the direct electron transfer from PSI to TiO_2 occurs.[29] Therefore, we proposed to directly use chloroplast or TK, assembled PSI and PSII, as an oxygen producing photocatalytic material to develop an electrode with function

[a] Advanced Research Institute for Natural Science and Technology, Osaka City University, Sugimoto 3-3-138, Sumiyoshi-ku, Osaka 558-8585, Japan
[b] Research Center for Artificial Photosynthesis, Osaka City University, Sugimoto 3-3-138, Sumiyoshi-ku, Osaka 558-8585, Japan
[c] Department of Applied Chemistry, Oita University, Dannoharu 700, Oita 870-1192, Japan
[d] Precursory Research for Embryonic Science and Technology (PRESTO), Japan Science and Technology Agency, 4-1-8 Honcho Kawaguchi, Saitama 332-0012, Japan
See DOI: 10.1039/x0xx00000x

of PSII. We also reported a photovoltaic conversion system based on the combination of oxygen production from water with chloroplast from spinach onto the nanocrystalline TiO_2 film electrode by irradiation, and electrochemical reduction of oxygen to water due to the catalytic activity of the platinum electrode. [32,33] Thus, the chloroplast and TK are attractive materials for assembling a photovoltaic conversion system using a water molecule as a redox electrolyte. In this system, PSII in the chloroplast or TK acts as an oxygen production catalyst with visible light irradiation.

CO_2 conversion to organic molecules using visible light irradiation is a lucrative technology for assembling an artificial photosynthesis device. Some studies on the visible-light driven CO_2 conversion to organic molecules such as formic acid and methanol, using an enzyme and photo-redox system have been reported.[34-37] We previously reported visible-light driven enzymatic formic acid production from CO_2 using formate dehydrogenase (FDH) via the reduction of methylviologen (MV^{2+}) by photosensitization of water-soluble zinc porphyrin or chlorophyll-*a*. [38-43] The visible-light driven electrochemical biofuel cell converting CO_2 to formic acid involves an FDH and viologen co-immobilized electrode, instead of platinum electrode in the photovoltaic conversion system, combined with chloroplast from *Spinach* immobilized onto nanocrystalline TiO_2 film electrode and platinum electrode.

Since TK of microalgae, that are active in water, are expected to be more stable in aqueous solution than that of green plant, such as *Spinach*, we focused on TK from microalgae *Spirulina platensis*. *Spirulina platensis* thrives at a pH around 8.5 and a temperature around 30 °C. *Spirulina* grows efficiently in water, so it is easier to handle as a photosynthetic materials than that of green plant, such as *Spinach*. As no chloroplast is formed in *Spirulina*, *Spirulina* itself acts as a function of chloroplast. For utilization of chloroplast as a photoanode in the photovoltaic conversion system, in the future, chloroplast must be purified from green plants using the centrifugation, but *Spirulina* directly can be used as a photoanode material. Thus, we devoted to photosynthesis organ in *Spirulina* in the visible-light driven electrochemical conversion system.

In this work, a new visible-light driven electrochemical biofuel cell consisting of TK from *Spirulina platensis* immobilized on nanocrystalline TiO_2 layer electrode (TK/TiO_2) as a photoanode, FDH-viologen (1-carboxyundecanoyl-1'-methyl-4,4'-bipyridiniumbromide, iodide; $CH_3V(CH_2)_9COOH$) co-immobilized electrode as a cathode, and CO_2-saturated buffer solution as the redox electrolyte was developed, as shown in Fig. 1.

The principle of visible-light driven electrochemical biofuel cell consisting of TK/TiO_2, FDH-$CH_3V(CH_2)_9COOH$ and CO_2-saturated buffer solution is as follows.

1) Oxygen evolution with PSII in TK/TiO_2 occurs with visible-light irradiation.
2) The electron transfers from TK to the conduction band of TiO_2.
3) The electron transfers from TK/TiO_2 to FDH-$CH_3V(CH_2)_9COOH$ electrode though the external circuit.
4) Single-electron reduction of viologen moiety of $CH_3V(CH_2)_9COOH$ on electrode occurs.
5) CO_2 reduction to formic acid with the function of FDH catalytic activity with single-electron reduced viologen moiety as a co-enzyme onto FDH-$CH_3V(CH_2)_9COOH$ electrode proceeds.

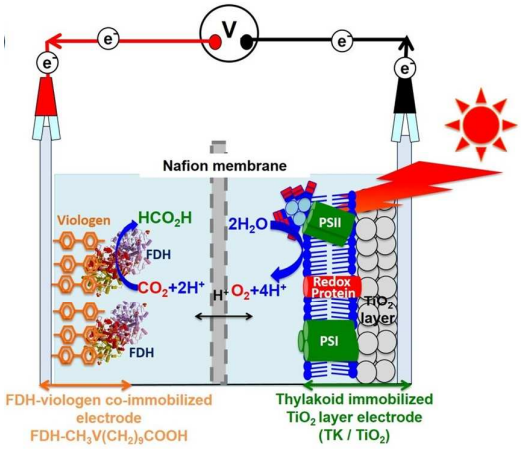

Figure 1. A visible-light driven electrochemical biofuel cell consisting of TK from microalgae *Spirulina platensis* immobilized on nanocrystalline TiO_2 layer electrode (TK/TiO_2) as a photoanode, FDH-viologen co-immobilized electrode (FDH-$CH_3V(CH_2)_9COOH$) as a cathode, and CO_2-saturated buffer solution as the redox electrolyte.

Results and discussion

Characterization of TK/TiO_2

UV-vis absorption spectrum of TK/TiO_2 is shown in Fig. 2 (solid line). As shown in Fig. 2, the absorption maxima are observed at 440, 490, 620 and 680 nm. In contrast, the absorption maxima of TK dispersed in a solution also are observed at 440, 490, 620 and 680 nm as shown in Fig. 2 (dash line).

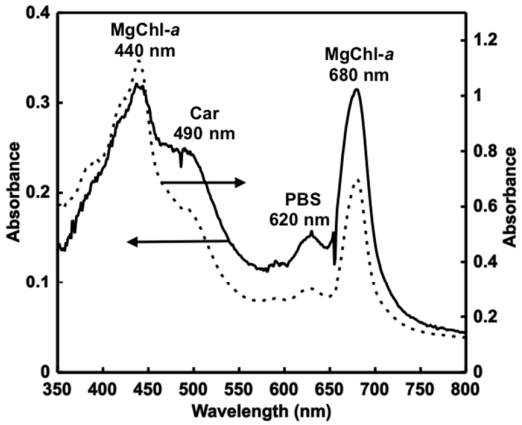

Figure 2. UV-vis absorption spectra of TK/TiO_2 (solid line) and TK dispersed in a solution (dash line).

The UV-vis absorption spectrum of TK/TiO_2 is similar to that of TK dispersed in a solution. The absorption band at 680 nm is

attributed to Mg chlorophyll-*a* (MgChl-*a*) (Q-band) along with its Soret band at 440 nm. The shoulder band at 490 nm is attributed to carotenoid (Car) absorption.[44,45] Presence of light harvesting site based on phycobilisomes (PBS) is observed at 620 nm absorption band. Thus, TK is immobilized onto TiO_2 film electrode.

The photosynthetic dyes such as MgChl-*a* fully were desorbed by immersing the TK is immobilized onto TiO_2 film electrode in acetone. After immersing the electrode in acetone, the amount of MgChl-*a* was determined with the molar coefficient (ε_{663} = 8.13 × 10^4 M^{-1} cm^{-1}) using UV-vis absorption spectroscopy. From the result of UV-vis absorption spectroscopy, the amount of adsorbed MgChl-*a* in TK/TiO_2 film electrode was estimated to be 14.8 nmol cm^{-2}. The ratio of MgChl-*a* contained in PSI and PSII was reported to be 94.5 to 5.5, respectively.[45] It has been reported that 920 molecules of MgChl-*a* were contained in one unit of the PSII.[44] Thus, the amount of PSII (0.86 nmol of MgChl-*a* cm^{-2}) in TK/TiO_2 film electrode were estimated to be 2.9 ×10^{12} units cm^{-2} (*ca.* 5.0 × 10^{-12} mol cm^{-2}). For PSII/benzoquinone polymer-based photo-bioelectrical cell, the amount of PSII onto electrode was estimated to be 1.5 × 10^{-12} mol cm^{-2}. In our system, as the TK was immobilized onto the electrode, the amount of PSII onto electrode was about 3.3 times compared with that of PSII/benzoquinone polymer-based photo-bioelectrical cell system.

To make sure the successful fabrication of TK/TiO_2 electrode, surface observation of the electrode was carried out using scanning electron microscopy (SEM). Fig. 3 show the photoimage and SEM image of TK/TiO_2 electrode and bare TiO_2 electrode.

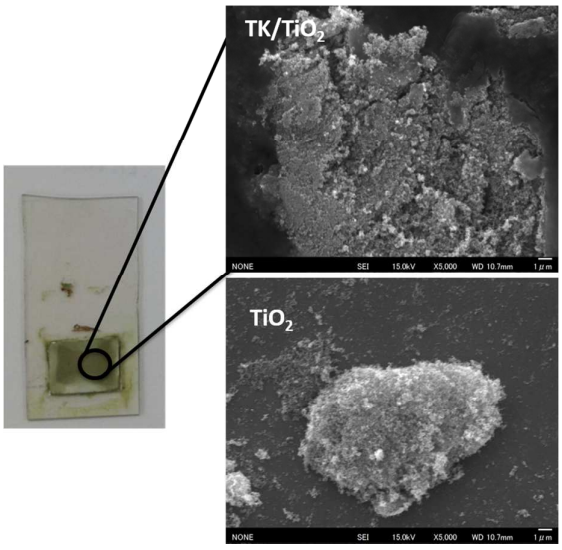

Figure 3. The photoimage, SEM images of TK/TiO_2 electrode and bare TiO_2 electrode.

From the result of SEM observation, it is not clear that TK immobilized onto TiO_2 electrode is formed, but it is estimated from the SEM images of the bare TiO_2 and TK/TiO_2 that a large TK covers the electrode surface. Thus, it was suggested that TK was immobilized onto TiO_2 electrode.

To confirm the successful fabrication of TK/TiO_2 electrode, photoelectrochemical properties of TK/TiO_2 electrode were studied using cyclic voltamogram (CV) under dark and visible-light irradiation.

Fig. 4 shows the representative CV under dark and visible-light irradiation of TK/TiO_2 electrode in the aqueous solution of sodium pyrophosphate buffer (50 mM, pH 7.4) containing 0.1 mM KCl at the scan rate of 10 mVs^{-1} (vs. Ag/AgCl (1 M KCl). The reversible redox curve is identifiable in all CV curves at a central potential of around 0.35 V for thylakoid electrochemistry. From CV curves in Fig. 4, the anodic current based on water oxidation of TK/TiO_2 electrode was observed with light irradiation. Thus, TK was immobilized onto TiO_2 electrode and TK/TiO_2 has sufficient oxygen production activity.

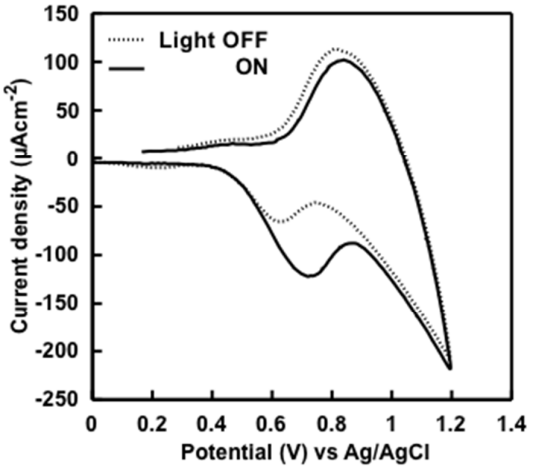

Figure 4. Representative CV of TK/TiO_2 electrode under dark and visible-light irradiation. Buffer solution: Sodium pyrophosphate buffer (50 mM, pH 7.4) containing 0.1 mM KCl; Scan rate: 10 mV s^{-1}.

Oxygen production activity of TK/TiO_2 under visible-light irradiation

To confirm the oxygen evolved complex (OEC) activity of TK/TiO_2 in CO_2-saturated buffer solution under visible-light irradiation, oxygen production of TK/TiO_2 under 100 $mWcm^{-2}$ light irradiation in the presence of dichloroindophenol (DCPIP) as a sacrificial oxidant is studied in the nitrogen-saturated (closed circle) or CO_2-saturated (open square) 50 mM sodium pyrophosphate buffer (pH 7.4) as shown in Fig. 3. In all experiments, to prevent degradation of TK and direct excitation of TiO_2 by near UV light, wavelengths of less than 390 nm were blocked with a cut-off filter (SCF-50S-39L Sigma Koki). In both cases, oxygen production was observed with irradiation time. This result indicates that CO_2 has no effect on oxygen production activity of TK/TiO_2. In contrast, no oxygen production was observed in the absence of DCPIP (×) or dark condition (open circle). Thus, the oxygen was produced with the photocatalytic function of TK/TiO_2 under visible-light

irradiation. Oxygen production activity of TK/TiO_2 was estimated to be 30 nmol cm^{-2} min^{-1}. The turnover number of PSII in TK/TiO_2 in the presence of DCPIP was estimated to be 1.5×10^4 min^{-1}.

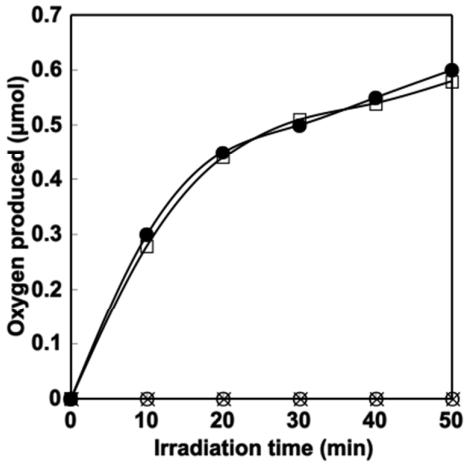

Figure 5. Time dependence of oxygen production of TK/TiO_2 under 100 $mWcm^{-2}$ light irradiation in the presence of DCPIP in the nitrogen-saturated (closed circle) or CO_2-saturated (open square) 50 mM sodium pyrophosphate buffer (pH 7.4)

From these results, it was suggested that TK/TiO_2 has sufficient oxygen production activity even in CO_2-saturated buffer solution as an electrode. Furthermore, oxygen production from TK/TiO_2 was observed even under visible-light while applying a bias equal to or lower than the oxidation potential of water. Thus, the successful fabrication of TK/TiO_2 electrode was made sure from these experimental results.

Characterization of FDH-$CH_3V(CH_2)_9COOH$ electrode

UV-vis absorption spectrum of $CH_3V(CH_2)_9COOH$/ITO electrode is shown in Fig. 6 (solid line). As shown in Fig. 6, the absorption maximum is observed at 270 nm. In contrast, the absorption maximum of $CH_3V(CH_2)_9COOH$ in a methanol solution also is observed at 265 nm as shown in Fig. 6 (dash line).

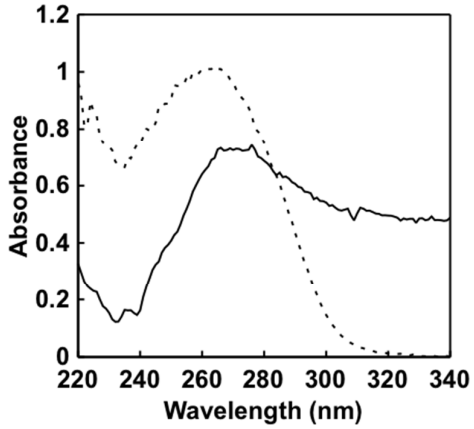

Figure 6. UV-vis absorption spectra of $CH_3V(CH_2)_9COOH$/ITO electrode (solid line) and $CH_3V(CH_2)_9COOH$/ITO in a methanol solution (dash line).

The UV-vis absorption spectrum of $CH_3V(CH_2)_9COOH$/ITO electrode is similar to that of $CH_3V(CH_2)_9COOH$ in a methanol solution. Thus, $CH_3V(CH_2)_9COOH$ is immobilized onto ITO electrode.

The amount of $CH_3V(CH_2)_9COOH$ immobilization onto ITO electrode was estimated to be 280 ± 10 nmol cm^{-2} using a spectrophotometer. The amount of FDH in FDH-$CH_3V(CH_2)_9COOH$ was calculated using enzyme activity assay and was estimated to be *ca.* 97.5 nmol cm^{-2}.

To make sure the successful fabrication of FDH-$CH_3V(CH_2)_9COOH$ electrode, surface observation of the electrode was carried out using scanning electron microscopy (SEM). Figure 7 show the photoimage and SEM image of $CH_3V(CH_2)_9COOH$/ITO electrode and FDH-$CH_3V(CH_2)_9COOH$ electrode.

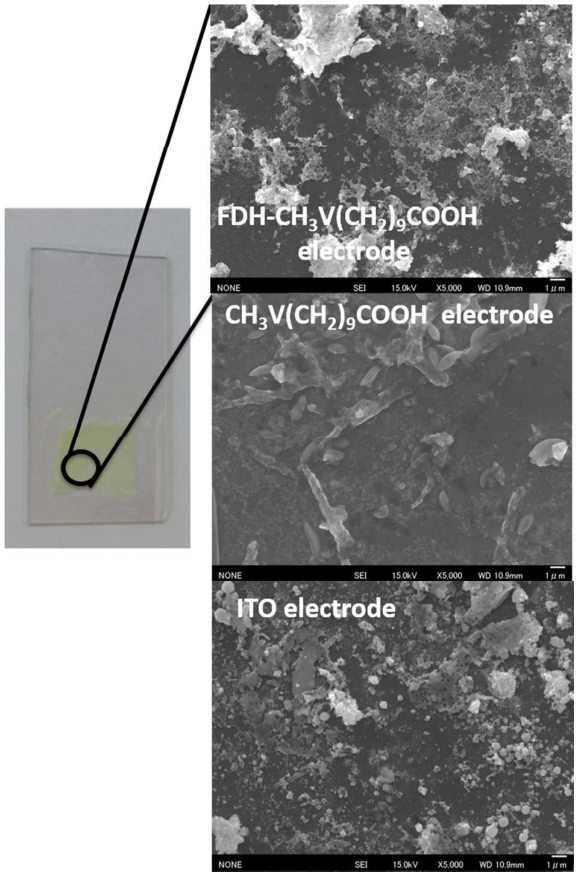

Figure 7. The photoimage, SEM images of bare ITO electrode, $CH_3V(CH_2)_9COOH$/ITO electrode and FDH-$CH_3V(CH_2)_9COOH$ electrode.

From the result of SEM observation, it is not clear that FDH immobilized onto $CH_3V(CH_2)_9COOH$/ITO electrode is formed, but it is estimated from the SEM images of the bare ITO, $CH_3V(CH_2)_9COOH$/ITO, and FDH-$CH_3V(CH_2)_9COOH$ electrodes that a large FDH covers the electrode surface.

To confirm the successful fabrication of FDH-$CH_3V(CH_2)_9COOH$ electrode, electrochemical properties of FDH-$CH_3V(CH_2)_9COOH$ electrode were studied using CV. Figure 8 shows the CV of $CH_3V(CH_2)_9COOH$/ITO (dotted line) and FDH-$CH_3V(CH_2)_9COOH$ (solid line) electrodes in aqueous solution of the CO_2 saturated sodium pyrophosphate buffer (50 mM, pH

7.4) containing 0.1 mM KCl at the scan rate of 10 mVs^{-1} (vs. Ag /AgCl (1 M KCl)) as an example.

In both case of $CH_3V(CH_2)_9COOH$/ITO and FDH-$CH_3V(CH_2)_9COOH$ electrodes, the shape of CV was almost the same. The potential due to the single-electron reduced viologen moiety was estimated to be -550 ± 5 mV in the $CH_3V(CH_2)_9COOH$ /ITO and FDH-$CH_3V(CH_2)_9COOH$ electrodes. This value is almost equal to that in the $CH_3V(CH_2)_9COOH$ solution. Figure 8 also shows the image of surface colour change of $CH_3V(CH_2)_9COOH$/ITO and FDH-$CH_3V(CH_2)_9COOH$ electrodes in aqueous solution of CO_2 saturated sodium pyrophosphate buffer (50 mM, pH 7.4) containing 0.1 mM KCl under the application of -550 mV potential vs. Ag/AgCl (1 M KCl) for 2 h. The colour of surface of $CH_3V(CH_2)_9COOH$/ITO or FDH-$CH_3V(CH_2)_9COOH$ electrodes was changed to blue with potential application, indicating the single-electron reduction of viologen moiety onto the electrode.

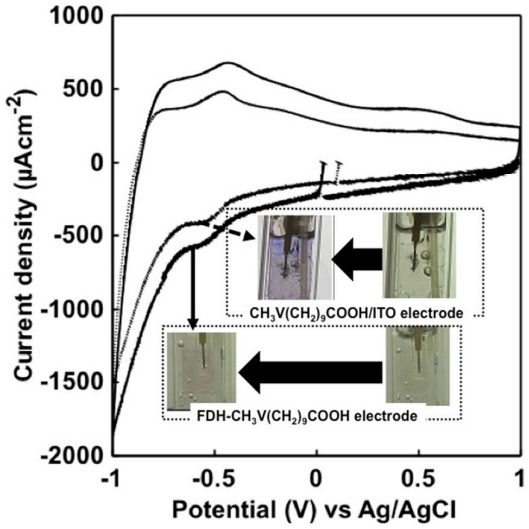

Figure 8. Representative CV of $CH_3V(CH_2)_9COOH$/ITO (dotted) and FDH-$CH_3V(CH_2)_9COOH$ (solid) electrodes. Buffer solution: CO_2 saturated sodium pyrophosphate buffer (50 mM, pH 7.4) containing 0.1 mM KCl; Scan rate: 10 mV s^{-1}. Inset: The colour changes of $CH_3V(CH_2)_9COOH$/ITO and FDH-$CH_3V(CH_2)_9COOH$ electrode surface in aqueous solution of CO_2 saturated sodium pyrophosphate buffer (50 mM, pH 7.4) containing 0.1 mM KCl under the application of -550 mV potential vs. Ag/AgCl (1 M KCl) for 2 h

From CV curves in Fig. 8, the cathodic current in FDH-$CH_3V(CH_2)_9COOH$ electrode was increased compared with that of $CH_3V(CH_2)_9COOH$/ITO electrode. Thus, TK was immobilized onto TiO_2 electrode and TK/TiO_2 has sufficient oxygen production activity. These results indicate the catalytic current based on the CO_2 reduction to formic acid with FDH on the electrode. From the observation of colour changes of $CH_3V(CH_2)_9COOH$/ITO or FDH-$CH_3V(CH_2)_9COOH$ electrodes surfaces, the viologen moiety of $CH_3V(CH_2)_9COOH$/ITO electrode was more single-electron reduced compared with that of FDH-$CH_3V(CH_2)_9COOH$ electrode. By immobilized FDH on the electrode, it is shown that single-electron reduced viologen moiety on the electrode acts as a co-enzyme for FDH and is used for CO_2 reduction to formic acid.

Figure 9 shows the time dependence of absorption changes at 570 nm due to the single-electron reduced viologen moiety on $CH_3V(CH_2)_9COOH$/ITO (closed circle) and FDH-$CH_3V(CH_2)_9COOH$ (open circle) electrodes under the bias application of -550 mV potential vs. Ag/AgCl (1 M KCl).

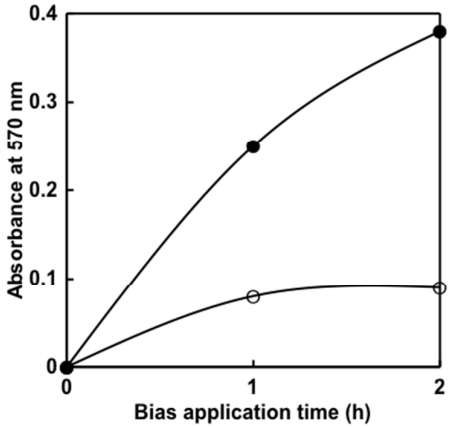

Figure 9. Time dependence of absorption changes at 570 nm due to the single-electron reduced viologen moiety on $CH_3V(CH_2)_9COOH$/ITO (closed circle) and FDH-$CH_3V(CH_2)_9COOH$ (open circle) electrodes under the bias application of -550 mV potential vs. Ag/AgCl (1 M KCl) in 50 mM sodium pyrophosphate buffer (pH 7.4)

From results of Fig. 9, the viologen moiety of $CH_3V(CH_2)_9COOH$/ITO electrode was more single-electron reduced compared with that of FDH-$CH_3V(CH_2)_9COOH$ electrode. As the single-electron reduction of viologen moiety onto FDH-$CH_3V(CH_2)_9COOH$ electrode was accomplished, the electrochemical CO_2 reduction to formic acid was attempted. Fig. 10 shows the time dependence of formic acid produced using FDH-$CH_3V(CH_2)_9COOH$ electrode in CO_2 saturated sodium pyrophosphate buffer (50 mM, pH 7.4) containing 0.1 mM KCl under the application of -550 mV potential vs. Ag/AgCl (1 M KCl)

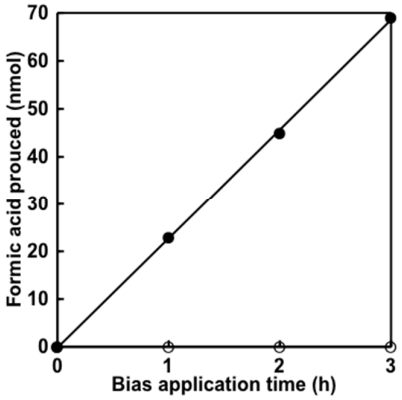

Figure 10. Time dependence of formic acid production with $CH_3V(CH_2)_9COOH$/ITO (closed circle) and FDH-$CH_3V(CH_2)_9COOH$ (open circle) electrodes under the bias application of -550 mV potential vs. Ag/AgCl (1 M KCl) in CO_2 saturated 50 mM sodium pyrophosphate buffer (pH 7.4)

By using FDH-$CH_3V(CH_2)_9COOH$ electrode, the amount of formic acid was increased with increasing bias application time. On the other hand, no formic acid production was observed with $CH_3V(CH_2)_9COOH$/ITO electrode. Moreover, formic acid production was observed with $CH_3V(CH_2)_9COOH$/ITO electrode in addition of FDH into CO_2 saturated sodium pyrophosphate buffer under bias application. No formic acid production also was observed with only FDH immobilized ITO electrode under bias application. From these results, both viologen as a co-enzyme and FDH as a catalyst are required for electrochemical CO_2 reduction to formic acid.

Voltage response of TK/TiO_2 with visible-light irradiation

Fig. 11 shows the voltage response of TK/TiO_2 | FDH-$CH_3V(CH_2)_9COOH$ on 100 mWcm^{-2} irradiation. In all experiments, to prevent degradation of TK and direct excitation of TiO_2 by near UV light, wavelengths of less than 390 nm were blocked with a cut-off filter.The voltage increased on irradiation and decreased under dark conditions. The light and dark voltages were estimated to be 570 and 0.1 mV, respectively. In the TK/TiO_2|FDH-$CH_3V(CH_2)_9COOH$, the electrolyte consisted of only the CO_2-saturated 50 mM sodium pyrophosphate buffer (pH 7.4) containing 0.1 mM KCl. The photovoltage was estimated to be 569 mV under the irradiation.

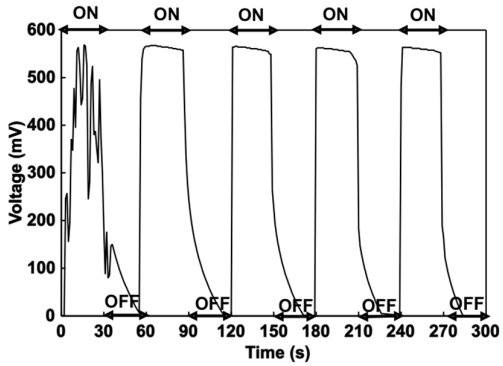

Figure 11. Voltage responses of TK/TiO_2 | FDH-$CH_3V(CH_2)_9COOH$ under dark and irradiation cycles with 100 mWcm^{-2} light.

Current response of TK/TiO_2 with visible-light irradiation

Fig. 12 shows the current response of TK/TiO_2 | FDH-$CH_3V(CH_2)_9COOH$ on 100 mWcm^{-2} irradiation. The current increased on irradiation and decreased under dark conditions. The light and dark currents were estimated to be 55 ± 10 and 5.0 ± 5 μA cm^{-2}, respectively. In the TK/TiO_2|FDH-$CH_3V(CH_2)_9COOH$, the electrolyte consisted of only the CO_2-saturated 50 mM sodium pyrophosphate buffer (pH 7.4). The photocurrent was estimated to be 50 ± 5 μA cm^{-2} under the irradiation. For TK/TiO_2 | FDH-$CH_3V(CH_2)_9COOH$, in contrast, no oxygen reduction process is needed and CO_2 reduction to formic acid onto FDH-$CH_3V(CH_2)_9COOH$ using H^+ and electron produced from TK/TiO_2. For TK/TiO_2 | FDH-$CH_3V(CH_2)_9COOH$, the two electrodes were separated by the Nafion 115 membrane. The Nafion 115 membrane was treated with sulfuric acid so as to stably and efficiently exhibit H^+ permeability function in aqueous solution.

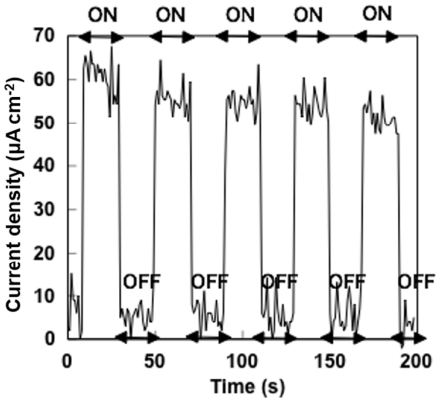

Figure 12. Current responses of TK/TiO_2 | FDH-$CH_3V(CH_2)_9COOH$ under dark and irradiation cycles with 100 mWcm^{-2} light.

The ohmic resistance of Nafion 115 membrane was estimated to be 1.3 × 10^6 Ω cm^{-2} in this system using electrochemical procedure. The ionic conductivity of Nafion 115 membrane was estimated to be 1.5 x 10^{-2} Ω^{-1} cm^{-1}. These results suggested that some impedance loss in this cell will occur. In the case of TK/TiO_2 | FDH-$CH_3V(CH_2)_9COOH$ without Nafion 115 membrane, however, the oxygen produced from TK/TiO_2 acted as a scavenger for the reduced form of viologen moiety in FDH-$CH_3V(CH_2)_9COOH$. Thus, the cell performance drastically was decreased and no formic acid production was observed under irradiation. As there were some impedance loss using Nafion 115 membrane in the cell, to prevent oxygen transferring to FDH-$CH_3V(CH_2)_9COOH$ side, Nafion 115 membrane was needed to the cell.

Dark and light current and potential curves for TK/TiO_2|FDH-$CH_3V(CH_2)_9COOH$ using linear polarization

Fig. 13 shows dark and light current and potential (*J*-*V*) curves for TK/TiO_2 | FDH-$CH_3V(CH_2)_9COOH$, respectively.

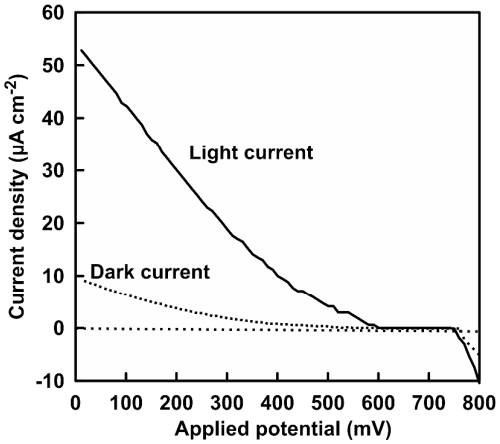

Figure 13. Dark and light current and potential (*J*-*V*) curves of TK/TiO_2 | FDH-$CH_3V(CH_2)_9COOH$ with 100 mWcm^{-2} light.

For TK/TiO_2 | FDH-$CH_3V(CH_2)_9COOH$, V_{oc} and J_{sc} in light current were estimated to be 600 mV and 54.5 μAcm^{-2}, respectively. In dark current, V_{oc} and J_{sc} were estimated to be 598 mV and 10.0 μAcm^{-2}, respectively. Thus, actual J_{sc} in photocurrent was estimated to be 44.5 μAcm^{-2}.

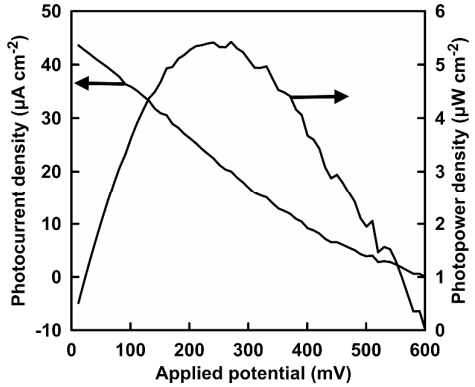

Figure 14. Photocurrent and photopower as a function of applied potential in TK/TiO_2 | FDH-$CH_3V(CH_2)_9COOH$ .with 100 mWcm^{-2} light.

V_{oc} and J_{sc} values in light and dark current obtained by LP measurements were in good agreement with the result of current and voltage responses with the cycles of dark/ irradiation of 100 mWcm^{-2} light.

Fig. 14 shows the photocurrent density and photopower density as a function of applied potential in TK/TiO_2 | FDH-$CH_3V(CH_2)_9COOH$. Here, photocurrent was calculated by subtracting dark current from light current. Photopower density is calculated by $P = J\,V$.

From these results, the maximum of photopower of TK/TiO_2 | FDH-$CH_3V(CH_2)_9COOH$ was estimated to be 5.3 μWcm^{-2} (V=286 mV), respectively. The data of photocurrent, photovoltage and photopower obtained from the cycles of dark/ irradiation of 100 mWcm^{-2} light and LP measurements were summarised in Table 1.

Table 1. *J–V* characteristics for TK/TiO_2 | FDH-$CH_3V(CH_2)_9COOH$ obtained from the cycles of dark/ irradiation of 100 mWcm^{-2} light and LP measurements

			TK/TiO_2 | FDH-$CH_3V(CH_2)_9COOH$
Dark/ irradiation cycles	Light current	V_{oc} (mV)	570
		J_{sc} (μAcm^{-2})	55 ± 10
	Dark current	V_{oc} (mV)	0.1
		J_{sc} (μAcm^{-2})	5.0 ± 5
	photocurrent	J_{sc} (μAcm^{-2})	50 ± 5
LP	Light current	V_{oc} (mV)	600
		J_{sc} (μAcm^{-2})	54.5
	Dark current	V_{oc} (mV)	598
		J_{sc} (μAcm^{-2})	10.0
	photocurrent	J_{sc} (μAcm^{-2})	44.5
	Photopower	P_{max} (μWcm^{-2})	5.3

Photocurrent action spectrum of TK/TiO_2|FDH-$CH_3V(CH_2)_9COOH$

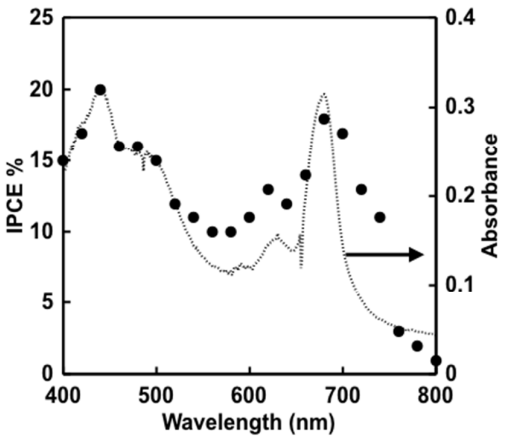

Figure 15. Photocurrent action spectrum of TK/TiO_2|FDH-$CH_3V(CH_2)_9COOH$ (circle) and UV-vis absorption spectrum of TK/TiO_2 (dotted line).

Fig. 15 shows the photocurrent action spectrum of TK/TiO_2|FDH-$CH_3V(CH_2)_9COOH$ (circle), where the incident photon to current conversion efficiency (IPCE) is plotted as a function of wavelength. The maximum peaks of UV-vis absorption spectrum of TK/TiO_2 are 440, 490, 620 and 680 nm as shown in Figs. 2 and 15. The maximum peaks of photocurrent action spectrum of the TK/TiO_2|FDH-$CH_3V(CH_2)_9COOH$ also are 440, 490, 620 and 680 nm and IPCE values at 440, 620 and 680 nm are estimated to be *c.a* 20, 14 and 19 %, respectively. From UV-vis absorption spectrum of TK/TiO_2 and photocurrent action spectrum of the TK/TiO_2|FDH-$CH_3V(CH_2)_9COOH$, the shape of both spectra were similar as shown in Fig. 15. Thus, photon-to-current conversion proceeded based on the function of TK onto TiO_2 electrode.

Formic acid production in the TK/TiO_2|FDH-$CH_3V(CH_2)_9COOH$ on visible-light irradiation

Next, we focused on formic acid production from CO_2 in the TK/TiO_2|FDH-$CH_3V(CH_2)_9COOH$ on irradiation with visible-light. Fig. 16 shows the time dependence of photocurrent of TK/TiO_2|FDH-$CH_3V(CH_2)_9COOH$ with continuous 100 mWcm^{-2} irradiation. In all experiments, to prevent degradation of TK and direct excitation of TiO_2 by near UV light, wavelengths of less than 390 nm were blocked with a cut-off filter. The volumes of electrolyte and gaseous phase in the anode and cathode sides were 0.5 mL, respectively. The distance between the working and counter electrode was 0.5 cm.

The photocurrent generated during a continuous irradiation was estimated to be 55 ± 10 μA cm^{-2}. Fig. 17 shows the time dependence of formic acid and oxygen production in the TK/TiO_2|FDH-$CH_3V(CH_2)_9COOH$ on continuous visible-light irradiation. The amounts of formic acid and oxygen were increased with increasing irradiation time. After 3 h irradiation, the amounts of formic acid and oxygen produced in the TK/TiO_2|FDH-$CH_3V(CH_2)_9COOH$ were estimated to be 30.0 and 12.5 nmol, respectively.

In Fig. 17, the time dependence of the amount of hydrogencarbonate (HCO_3^-) also is indicated. Before irradiation, the concentration of HCO_3^- in a sample CO_2 saturated sodium pyrophosphate buffer was estimated to be 7.0 mM (3.5 μmol) by an ion chromatography system. In solution, FDH catalyzes the reduction of HCO_3^- to formic acid rather than directly CO_2 reduction. Therefore, the decrease in HCO_3^- and the increase in formic acid are interlocked. Frome the results of Fig. 17, as the amount of HCO_3^- decreases, the amount of formic acid produced increases with irradiation time.

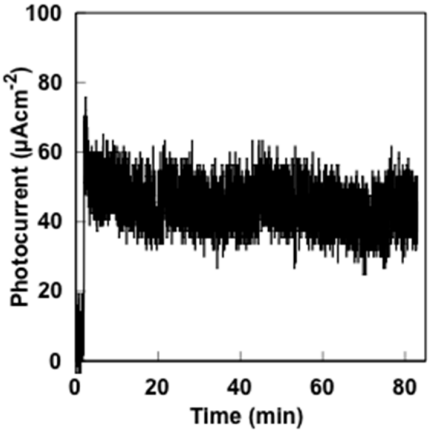

Figure 16. Time dependence of photocurrent generation in the visible-light driven electrochemical biofuel cell consisting of TK/TiO_2 and FDH-$CH_3V(CH_2)_9COOH$ electrodes under continuous irradiation with 100 $mWcm^{-2}$ light.

On the contrary, formic acid and oxygen were not produced under dark conditions. The mechanism of photocurrent generation and formic acid and oxygen production in TK/TiO_2|FDH-$CH_3V(CH_2)_9COOH$ on continuous irradiation is as follows. Initially, the PSII in TK/TiO_2 was excited by irradiation with visible light, thus producing oxygen. Then, an electron was transferred from the TK to the conduction band of TiO_2, followed by transfer to the viologen moiety, and lastly to the FDH moiety in FDH-$CH_3V(CH_2)_9COOH$ electrode. Finally, CO_2 in the electrolyte was reduced to formic acid by the catalytic activity of FDH onto FDH-$CH_3V(CH_2)_9COOH$ electrode. The ratio of formic acid to oxygen production in TK/TiO_2|FDH-$CH_3V(CH_2)_9COOH$ on continuous irradiation was estimated to be ~2. Thus, formic acid and oxygen were produced stoichiometrically in this visible-light driven electrochemical biofuel cell. The turnover number of PSII in TK/TiO_2 in this visible-light driven electrochemical biofuel cell was estimated to be *ca.* 2777 h^{-1}.

On the other hand, the amount of FDH in FDH-$CH_3V(CH_2)_9COOH$ was calculated using enzyme activity assay and was estimated to be *ca.* 97.5 nmol cm^{-2}. The turnover number of FDH in FDH-$CH_3V(CH_2)_9COOH$ was calculated to be *ca.* 0.3 h^{-1}. In CO_2 saturated 50 mM sodium pyrophosphate buffer containing 0.1 mM KCl, FDH catalyzes the reduction of HCO_3^- to formic acid. Before irradiation, the concentration of HCO_3^- in a sample CO_2 saturated sodium pyrophosphate buffer was estimated to be 3.5 μmol by an ion chromatography system. As the volume of aqueous media was 0.5 mL, the conversion yield of CO_2 to formic acid in TK/TiO_2|FDH-$CH_3V(CH_2)_9COOH$ was estimated to be *ca*. 0.85%.

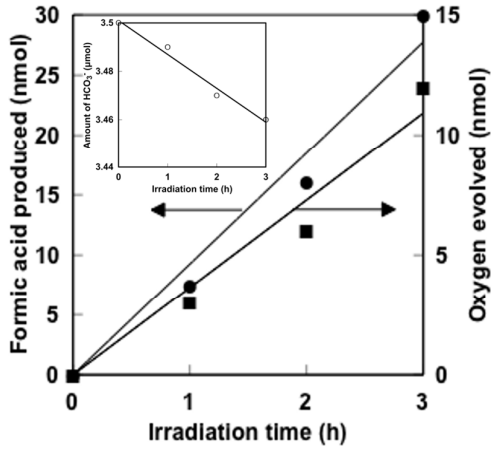

Figure 17. Time dependence of formic acid and oxygen production in the visible-light driven electrochemical biofuel cell consisting of TK/TiO_2 and FDH-$CH_3V(CH_2)_9COOH$ electrodes under continuous irradiation with 100 $mWcm^{-2}$ light. Inset: Time dependence of the amount of HCO_3^- in the visible-light driven electrochemical biofuel cell.

By using bare TiO_2|FDH-$CH_3V(CH_2)_9COOH$, no formic acid and oxygen production were observed under continuous 100 $mWcm^{-2}$ irradiation with a cut-off filter (less than 390 nm). On contrast, formic acid production was observed by using bare TiO_2|FDH-$CH_3V(CH_2)_9COOH$ under the UV-light irradiation (Xe-lamp). No formic acid production was observed in the absence of CO_2, TK/TiO_2|FDH (without $CH_3V(CH_2)_9COOH$), or TK/TiO_2|$CH_3V(CH_2)_9COOH$ (without FDH) under continuous 100 $mWcm^{-2}$ irradiation. Thus, all of TK, TiO_2, FDH and $CH_3V(CH_2)_9COOH$ are required to develop the visible-light driven electrochemical biofuel cell with the function of CO_2 conversion to formic acid.

In addition, as a result of investigating the influence of the distance between the TK/TiO_2 and FDH-$CH_3V(CH_2)_9COOH$ electrodes to the cell performance, photocurrent was observed, but the reduction efficiency of CO_2 decreased under the distance more than 1.5 cm between the TK/TiO_2 and FDH-$CH_3V(CH_2)_9COOH$ electrodes.

Although highly phoelectrochemical conversion efficiency using the purified-photosynthetic protein such as PSI, PSII immobilized electrode was achieved, the stability against visible-light irradiation for a long period was hardly improved. As the membrane-bound proteins exert their function in the lipid bilayer membrane, in general, their stabilities decrease due to purified from the membrane. Activities of these membrane-bound proteins were reduced even in micelles formed with surfactants. In contrast, by using TK directly for visible-light driven electrochemical biofuel cell, photosynthetic proteins, PSI, PSII work in almost the same environment as nature, thus, PSII stably was functioned onto the TiO_2 electrode. Thus, a new biofuel cell system with functions of solar cell and CO_2 conversion was developed using TK/TiO_2|FDH-$CH_3V(CH_2)_9COOH$.

Mechanistic pathway for electron transfer in TK/TiO_2|FDH-$CH_3V(CH_2)_9COOH$

Fig. 18 shows the mechanistic pathway for visible-light driven electron transfer in TK/TiO_2|FDH-$CH_3V(CH_2)_9COOH$.

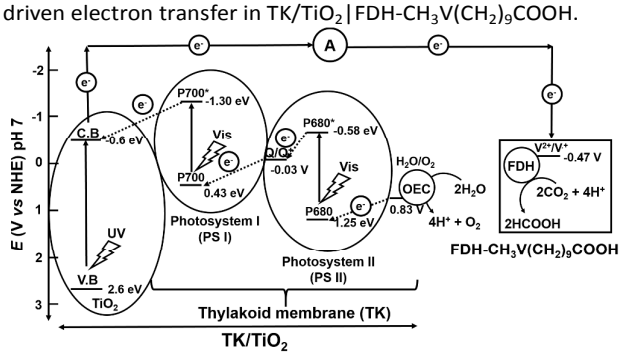

Figure 18. Energy diagram for the working mechanism and electron transfer pathway in the TK/TiO_2|FDH-$CH_3V(CH_2)_9COOH$ cell. Data from ref.51-55.

In this Figure, C.B and V.B represent the conduction and valance band of TiO_2, P700 and P700* represent lower and excited energy states of PSI respectively, P680 and P680* represent the lower and excited states of PSII respectively and Q represents quinone. OEC represents the oxygen-evolved complex, V represents the viologen moiety of FDH-$CH_3V(CH_2)_9COOH$. The band position values also were mentioned in the figure. The process starts at PSII, where the reaction center chlorophyll molecules in P680 harvest visible-light energy for charge separation. An electron from P680, the lower energy state in PSII is excited to the higher energy state, P680*. After subsequent transfer within PSII, the electron transfers to P700 in PSI, via intrinsic electron mediators such as quinones. A second electron excitation occurs at PSI and the electron moves to the excited state, P700*. After sequential electron transfer in PSI, the electron reaches the electron mediators such as ferredoxins in PSI, and then to the conduction band (C.B) of TiO_2 at a lower redox potential. From TiO_2, the electron transfers through the external circuit and reaches the FDH-$CH_3V(CH_2)_9COOH$ electrode, where it reduces viologen moiety of $CH_3V(CH_2)_9COOH$ and then CO_2 reduction to formic acid with the catalytic activity of FDH. The electron in PSII, is regenerated by the oxidation of water to oxygen with OEC as the redox potential of water oxidation is higher than that of P680. Thus, the cycle completes, producing oxygen at the working electrode (TK/TiO_2) and CO_2 reduction at the counter electrode (FDH-$CH_3V(CH_2)_9COOH$). In this scheme PSI alone cannot complete the cycle of electron transfer because of the absence of a sacrificial electron donor in the system. PSI cannot accept electrons from water attributed to the unfavorable energy level alignment, as the water oxidation potential is lower than that of P700, the lower energy state of PSI as explained in Fig. 18. The electron at PSI has to move from PSII. Simultaneously, PSII alone will also not work with TiO_2 because the conduction band of TiO_2 is higher potential than that of quinones in the electron transfer chain in PSII, disabling the direct electron transfer from PSII to TiO_2. From the Fig. 18, the photovoltaic system using the combination of Thylakoid membrane including PSI and PSII, and FDH-based electrodes would be operated without any bias voltage.

As mentioned above, all of TK, TiO_2, FDH and $CH_3V(CH_2)_9COOH$ are needed to develop the visible-light driven electrochemical biofuel cell with the function of CO_2 reduction to formic acid. Especially, PSII in TK with the function of water to photolysis into oxygen, and acquires electrons and protons with visible-light irradiation is the most important photoanode material. As the PSII purified from micro-algae is very unstable, however, stability against light irradiation for a long period and on the electrode are serious problems for the utilization of visible-light driven electrochemical biofuel cell. Therefore, direct utilization of TK assembled the photosynthetic proteins give important approach for device application of visible-light driven electrochemical biofuel cell.

Experimental

Materials

Spirulina platensis (NIES-39) was purchased from the National Institute for Environmental Studies. Titanium dioxide nano-powder (P25) was purchased from Degussa. Optical transparent conductive glass plate electrode (OTE) (10-15 Ω /square SnO_2: fluorine coated) was obtained from Nihon Sheet Glass Co. Ltd. Indium-tin oxide (ITO) nano-particle (particle shape: angular, average particle size: 30 nm) was obtained from C.I Kasei Co., Ltd. FDH from *Candida boidinii* and proton permeable membrane, Nafion® 115 film, was obtained from Sigma-Aldrich Co. Ltd. The other chemicals used were of analytical grade or the highest grade available.

1-Carboxyundecanoyl-1'-methyl-4,4'-bipyridiniumbromide, iodide ($CH_3V(CH_2)_9COOH$) was synthesized using a procedure described in the literature.[46-48] The Nafion® 115 film was treated with sulfuric acid before use for photochemical biofuel cell.

Isolation of TK from *Spirulina platensis*

Spirulina platensis was incubated in SOT culture medium et al., and TK was isolated using a previously described procedure.[49]

Preparation of nanocrystalline TiO_2 film electrode

The nanocrystalline TiO_2 film on ITO substrate was prepared using a procedure described previously.[50] TiO_2 powder was dispersed in concentrated nitric acid aqueous solution (pH=1.0). The viscous suspension was spread onto ITO (1 cm × 3 cm) at room temperature using scotch tape as a spacer. A thin film was obtained by raking off the excess suspension with a glass rod. After removing the tape, the plate was dried using a hot plate at 80 °C for 30 min, followed by annealing at 450 °C for 30 min under ambient conditions to form a nanocrystalline TiO_2 film onto the ITO substrate. The thickness of the film, determined by a micron-sensitive caliper, was approximately 10 μm. The active area of the electrode was 1.0 cm^2.

Preparation of TK- immobilized TiO_2 film electrode (TK/TiO_2)

TK-immobilized nanocrystalline TiO_2 layer on ITO glass substrate was prepared as follows: a nanocrystalline TiO_2 film on an ITO glass substrate was dipped into a TK suspension at 4 °C for 24 h. To prevent the TK on the electrode from eluting into the solution, the electrode surface was covered with polyion complex film consisting of poly-*L*-lysine and poly-L- TK-immobilized nanocrystalline TiO_2 film on ITO glass substrate is defined as TK/TiO_2 electrode. The surface structure of TK/TiO_2 electrode was observed using scanning electron microscopy (JSM-6500F FE-SEM JEOL). The CV curves under dark and visible-light irradiation of TK/TiO_2 electrode in the aqueous solution of sodium pyrophosphate buffer (50 mM, pH 7.4) containing 0.1 mM KCl at the scan rate of 10 mVs^{-1} (vs. Ag/AgCl (1 M KCl) were measured using potentiostat (Hokuto Denko HZ-3000). A solar simulator also was used as a light source (A.M. 1.5 100 mW cm^{-2}) with a cut-off filter (SCF-50S-39L Sigma Koki: less than 390 nm).

Preparation of FDH- and viologen-immobilized electrode (FDH-$CH_3V(CH_2)_9COOH$)

The FDH- and viologen-immobilized electrode was prepared using a modification of a previously described procedure. The viscous suspension containing indium-tin oxide (ITO) nanoparticle and polyethylene glycol was spread to 1 cm^2 onto an ITO glass substrate (1 × 5 cm) at room temperature. An ITO thin layer film was obtained by raking off the excess suspension with a glass rod. The substrate was dried using a hot plate at 80 °C for 30 min and annealed at 450 °C for 30 min under ambient conditions to form an ITO thin layer film electrode. The active area of electrode was 1.0 cm^2. To immobilize the 1-carboxyundecanoyl-1'-methyl-4,4'-bipyridinium bromide, iodide ($CH_3V(CH_2)_9COOH$) onto the ITO thin layer film electrode, the substrate was dipped into methanol solution containing $CH_3V(CH_2)_9COOH$ (300 μM) for 68 h at 25 °C. The electrode was washed with methanol to remove physically adsorbed $CH_3V(CH_2)_9COOH$. This electrode was defined as $CH_3V(CH_2)_9COOH$/ITO electrode. Finally, FDH was immobilized onto the $CH_3V(CH_2)_9COOH$/ITO electrode. The electrode was dipped into sodium pyrophosphate buffer solution (pH 7.4) containing FDH (0.75 μM) for 1 h at 4 °C, followed by washing with sodium pyrophosphate buffer solution (pH 7). To prevent $CH_3V(CH_2)_9COOH$ and FDH on the electrode from eluting into the solution, the electrode surface was covered with polyion complex film consisting of poly-*L*-lysine and poly-*L*-glutamine. This electrode was defined as FDH-$CH_3V(CH_2)_9COOH$ electrode. The surface structure of FDH-$CH_3V(CH_2)_9COOH$ electrode was observed using scanning electron microscopy. The CV curves FDH-$CH_3V(CH_2)_9COOH$ electrode and $CH_3V(CH_2)_9COOH$/ITO electrodes in the aqueous solution of CO_2 saturated sodium pyrophosphate buffer (50 mM, pH 7.4) containing 0.1 mM KCl at the scan rate of 10 mVs^{-1} (vs. Ag/AgCl (1 M KCl) were measured using potentiostat (Hokuto Denko HZ-3000). The concentration of formic acid produced in FDH-$CH_3V(CH_2)_9COOH$ with continues electrochemical bias application was measured using an ionic chromatograph system (Dionex IC2000). The other details of FDH-$CH_3V(CH_2)_9COOH$ electrode were reported previously.[47,48]

Oxygen production activity of TK/TiO_2 in the presence of DCPIP under visible-light irradiation

The oxygen production activity of PSII in TK/TiO_2 under the continuous visible-light irradiation in the presence of sacrificial reagent DCPIP was studied. The sodium pyrophosphate buffer (50 mM, pH 7.4) containing 0.3 mM of DCPIP was subjected to bubbling nitrogen or CO_2 gas for 20 min. The visible-light was irradiated to TK/TiO_2 in the sodium pyrophosphate buffer containing DCPIP. A solar simulator (YSS-40, Yamashita Denso) was used as a visible light source (A.M. 1.5 100 mW cm^{-2}). To prevent degradation of TK and direct excitation of TiO_2 by near UV light, wavelengths of less than 390 nm were blocked with a cut-off filter. The amount of oxygen produced was measured using the optical oxygen monitor (FireStingO2, Pyroscience).

Photocurrent action spectra measurement

A 400 W xenon lamp with a monochromator was used as light source for photocurrent action spectra measurements. The cell was operated in the short-circuit mode. Photocurrent action spectrum of TK/TiO_2|FDH-$CH_3V(CH_2)_9COOH$ was measured with a sandwich type cell. The working electrode with TK/TiO_2 was gently squeezed together with FDH-$CH_3V(CH_2)_9COOH$ as a counter electrode using spring and irradiated from the working electrode side. The sodium pyrophosphate buffer (50 mM, pH 7.4) containing 0.1 mM KCl was subjected to bubbling CO_2 gas for 20 min and then used as the electrolyte. The distance between the working and counter electrode was 0.5 cm. The incident photon-to-current conversion efficiency (IPCE) values were determined between 400 and 800 nm. The IPCE was then calculated according to the following equation:

$$IPCE = 1240\, J_{ph}(\mu A)/P(\mu W)\, \lambda\ (nm)$$

where J_{ph} and P are the photocurrent and power of the incident radiation per unit area and λ is the wavelength of the monochromatic light.

Characterization of visible-light driven electrochemical biofuel cell

The working electrode with TK/TiO_2 electrode was gently squeezed together with a FDH-$CH_3V(CH_2)_9COOH$ electrode as a counter electrode via the proton transparent membrane (PEM), Nafion® 115 using a spring and irradiated from the side of the working electrode. The sodium pyrophosphate buffer (50 mM, pH 7.4) containing 0.1 mM KCl was subjected to bubbling CO_2 gas for 20 min, and then used as the electrolyte. The volumes of electrolyte and gaseous phase in the anode and cathode sides were 0.5 mL, respectively. This visible-light driven electrochemical biofuel cell was defined as TK/TiO_2 | FDH-$CH_3V(CH_2)_9COOH$.

A solar simulator was used as a light source (A.M. 1.5 100 mW cm^{-2}) with a cut-off filter (less than 390 nm). The cell

was operated in the short-circuit mode. The voltage and current responses were measured using a digital multimeter (model 34401A, Agilent) under dark and irradiation cycles. The actual photocurrent was calculated from the difference in the curves. The active electrode area was 1.0 cm^2.

Linear polarization (LP) was used to obtain dark and light current–potential (*J–V*) curves for the visible-light driven electrochemical biofuel cells using potentiostat (Hokuto Denko HZ-3000) with sweep rate of 50 mV s^{-1}, and the photocurrent was calculated from the difference in the curves. In LP measurements, the potential between the anode and cathode was varied without a reference electrode, while current was monitored, allowing for probing of light and dark *J–V* characteristics of the visible-light driven electrochemical biofuel cells. A solar simulator also was used as a light source (A.M. 1.5 100 mW cm^{-2}) with a cut-off filter (less than 390 nm) for LP measurements. The active electrode area also was 1.0 cm^2 for LP measurements.

The concentration of formic acid produced and HCO_3^- in TK/TiO_2 | FDH-$CH_3V(CH_2)_9COOH$ during irradiation was measured using an ionic chromatograph system (Dionex IC2000). The amount of oxygen produced in the side of TK/TiO_2 was measured using the optical oxygen monitor.

Conclusions

In this work, development of a TK isolated from *Spirulina platensis* assembled onto TiO_2 film electrode, and its photon-to-current conversion function was studied. A visible-light driven electrochemical fuel cell, TK/TiO_2|FDH-$CH_3V(CH_2)_9COOH$, which converted CO_2 to formic acid, was also developed. The photovoltage and photocurrent of TK/TiO_2|FDH-$CH_3V(CH_2)_9COOH$ were responsive to visible-light on / off. The ratio of formic acid to oxygen production in TK/TiO_2|FDH-$CH_3V(CH_2)_9COOH$ on continuous irradiation was estimated to be ~2. Thus, formic acid and oxygen were produced stoichiometrically in this visible-light driven electrochemical biofuel cell. By using TK directly for visible-light driven electrochemical biofuel cell, PSI and PSII work in almost the same environment as nature, thus, the stable electrochemical cell using photosynthetic organs was accomplished. A new biocatalyst-fuel cell system with functions of a solar cell, reduction of CO_2, and lower carbon fuel production was developed in this study.

Acknowledgements

This work was partially supported by Precursory Research for Embryonic Science and Technology (PRESTO, Japan Science and Technology Agency JST). The authors would also like to express our gratitude to Prof. Tomoko Yoshida, Mr. Masato Akatsuka and Mr. Yuma Kato of Osaka City University for the SEM measurement of TK/TiO_2 and FDH-$CH_3V(CH_2)_9COOH$ electrodes.

Notes and references

1 K. Sauer and V. K. Yachandra, *Biochim. Biophys. Acta.* 2004, **1655**, 140.
2 B. Loll, J. Kern, W. Saenger, A. Zouni, J. Biesiadka, *Nature* 2005, 438, 1040.
3 Y. Taguchi and T. Noguchi, *Biochim. Biophys. Acta,* 2007, **1767**, 535.
4 M. Nagata, M. Nango, A. Kashiwada, S. Yamada, S. Ito, N. Sawa, M. Ogawa, K. Iida, Y. Kuronoa, and T. Ohtsuka, *Chem. Lett*. 2003, **32**, 216.
5 H. Krassen, A. Schwarze, B. Friedrich, K. Ataka, O. Lenz and J. Heberle, *ACS Nano*, 2009, **3**, 4055.
6 L. M. Utschig, N. M. Dimitrijevic, O. G. Poluektov, S. D. Chemerisov, K. L. Mulfort and D. M. Tiede, *J. Phys. Chem. Lett.,* 2011, **2**, 236.
7 F. Zhao, F. Conzuelo, V. Hartmann, H. Li, M. M. Nowaczyk, N. Plumeré, M. Rögner, and W. Schuhmann, *J. Phys. Chem. B.* 2015, **119**, 13726.
8 M. Ogawa, R. Kanda, T. Dewa, K. Iida, and M. Nango, *Chem. Lett*. 2002, **31**, 466.
9 M. Nango, A. Kashiwada, H. Watanabe, S. Yamada, M. Ogawa, T. Tanaka and K. Iida, *Chem. Lett*. 2002, **31**, 312.
10 Y. Amao, Y. Yamada, and K. Aoki, *J. Photochem. Photobiol. A: Chem.* 2004, **164**, 47.
11 Y. Amao, and T. Komori, *Biosens. Bioelectron*. 2004, 19, 843.
12 P. V. Kamat, J. P. Chauvet, and R.W. Fessenden, *J. Phys. Chem.* 1986, **90**, 1389.
13 A. Kay and M. Grätzel, *J. Phys. Chem.* 1993, **97**, 6272.
14 A. Kay, R. Humphry-Baker, and M. Grätzel, *J. Phys. Chem.* 1994, **98**, 952.
15 B.A. Kiselev and N-Y. Kozlo, *Bioelectrochemistry Bioenergetics* 1980, **7**, 247-254.
16 L.A. Khanova and M.R. Tarasevich, *J. Electroanal. Chem.* 1987, **227**, 115.
17 Y. Amao and Y. Yamada, *Langmuir* 2005, **21**, 3008.
18 Y. Amao and Y. Yamada, *Biosens. Bioelectron.* 2007, **22**, 1561.
19 M. Grätzel, *Nature* 1991, **414,** 338.
20 A. Hagfeldt and M. Grätzel, *Acc. Chem. Res.* 2000, **33**, 269.
21 K. Sayama, H. Sugihara, and H. Arakawa, *Chem. Mater.* 1998, **10**, 3825.
22 M. Nagata, M. Amano, T. Joke, K. Fujii, A. Okuda, M. Kondo, S. Ishigure, T. Dewa, K. Iida, F. Secundo, Y. Amao, H. Hashimoto, and M. Nango, *ACS Macro Letters,* 2012, **1**, 296.
23 M. Kato, T. Cardona, A.W. Rutherford, and E. Reisner, *J. Am. Chem. Soc.* 2012, **134**, 8332.
24 M. Kato, T. Cardona, A.W. Rutherford, and E. Reisner, *J. Am. Chem. Soc.* 2013, **135**, 10610.
25 J. Z. Zhang, K. P. Sokol, N. Paul, E. Romero, R. van Grondelle and E. Reisner, *Nat. Chem. Biol.* 2016, **12**,1049.
26 J. Li, X. Feng, J. Fei, P. Cai, Ji. Huang and J. Li. *J. Mater. Chem. A,* 2016,**4**, 12197.
27 J. Ihssen, A. Braun, G. Faccio, K. Gajda-Schrantz and L. Thöny-Meyer, *Curr. Protein Peptide Sci.* 2014, **15**,374.
28 Y. Zhang, N. M. Magdaong, M. Shen, H. A. Frank and J. F. Rusling, *ChemistryOpen*, 2015, **4**, 111.
29 O. Yehezkeli, R. Tel-Vered, D. Michaeli, R. Nechusthai and I. Willner, *Small* 2013, **9**, 2970.
30 A. Efrati, R. Tel-Vered, D. Michaeli, R. Nechusthai and I. Willner, *Energy Environ. Sci.* 2013, **6**, 2950.
31 O. Yehezkeli, R. Tel-Vered, J. Wasserman, A. Trifonv, D. Michaeli, R. Nechusthai and I. Willner, *Nature Commun.* 2012, **3**, 742
32 Y. Amao and A. Kuroki, *Electrochemistry,* 2009, **77**, 862.
33 Y. Amao, A. Tadokoro, M. Nakamura, N. Shuto, and A. Kuroki, *Res. Chem. Intermed.* 2014, **40**, 3257.
34 Y. Amao, *ChemCatChem*, 2011, **3**, 458.

35 D. Mandler and I. Willner, *J. Chem. Soc., Perkin Trans.*, 1988, **2**, 997.
36 I. Willner and D. Mandler, *J. Am. Chem. Soc.*, 1989, **111**, 1330.
37 I. Willner, N. Lapidot, A. Riklin, R. Kasher, E. Zahavy and E. Katz, *J. Am. Chem. Soc.*, 1994, **116**, 1428.
38 M. Kodaka and Y. Kubota, *J. Chem. Soc., Perkin Trans.*, 1999, **2,** 891.
39 R. Miyatani and Y. Amao, *Biotechnol. Lett*., 2002, **24,** 1931.
40 R. Miyatani and Y. Amao, *J. Mol. Catal. B. Enzym.*, 2004, **27**, 121.
41 R. Miyatani and Y. Amao, *J. Jpn. Petrol. Inst.*, 2004, **47**, 27.
42 I. Tsujisho, M. Toyoda and Y. Amao, *Catal. Commun*, 2006, **7**, 173.
43 T. Amao, R. Abe and S. Shiotani, *J. Photochem. Photobiol. A. Chem.,* 2015, **313**, 149.
44 M. Rakhimberdieva, V. A. Boichenko, N. V. Karapetyan and I. N. Stadnichuk, *Biochemistry,* 2001, **40**, 15780.
45 K. Verma and P. Mohanty, *Z. Naturforsch.* 2000, **55**, 16.
46 Y. Amao, N. Shuto, K. Furuno, A. Obata, Y. Fuchino, K. Uemura, T. Kajino, T. Sekito, S. Iwai, Y. Miyamoto and M. Matsuda, *Faraday Discuss.* 2012, **155,** 289.
47 Y. Amao and N. Shuto, *Res. Chem. Intermed.* 2014, **40**, 3267.
48 Y. Amao and N. Shuto, *J. Porphyrins Phthalocyanines* 2015, **19**, 459-464.
49 E. Šetlkov, D. Sofrova, V. Kovar and P. Budac, *Photosynthetica* 2013, **51**, 517.
50 S. Nakade, S. Kambe, T. Kitamura, Y. Wada and S. Yanagida, *J. Phys. Chem. B.* 2001, **105**, 9150
51 S. Kavadiya, T. S. Chadha, H. Liu, V. B. Shah, R. E. Blankenship and P. Biswas, *Nanoscale*, 2016, **8**, 1868.
52 R. E. Blankenship, Molecular mechanisms of photosynthesis, John Wiley & Sons, 2013.
53 V. B. Shah, W. R. Henson, T. S. Chadha, G. Lakin, H. Liu, R. E. Blankenship and P. Biswas, *Langmuir*, 2015, **31**, 1675.
54 M. Bledowski, L. Wang, A. Ramakrishnan, O. V. Khavryuchenko, V. D. Khavryuchenko, P. C. Ricci, J. Strunk, T. Cremer, C. Kolbeck and R. Beranek, *Phys.Chem.Chem.Phys.,* 2011, 13, 21511.
55 N. D. Kirchhofer, M. A. Rasmussen, F. W. Dahlquist, S. D. Minteer and G. C. Bazan, *Energy Environ. Sci.,*2015, **8**, 2698.

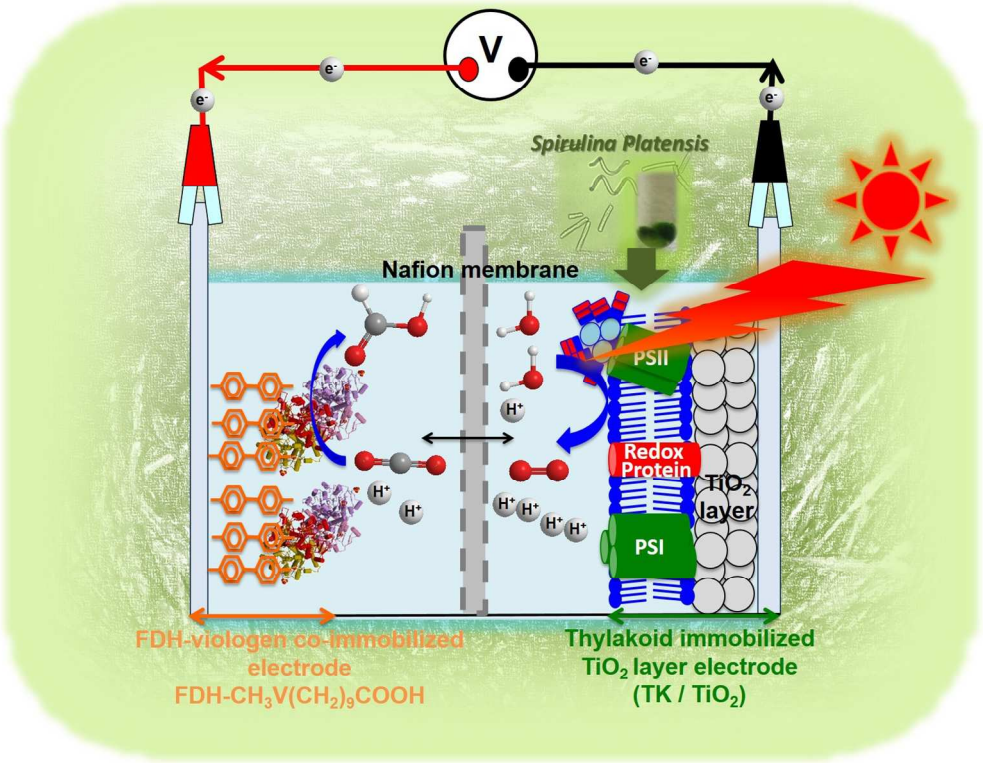

271x212mm (150 x 150 DPI)